











# Tomato *CRABS CLAW* paralogues interact with chromatin remodelling factors to mediate carpel development and floral determinacy

Laura Castañeda<sup>1</sup> , Estela Giménez<sup>1</sup> , Benito Pineda<sup>2</sup> , Begoña García-Sogo<sup>2</sup>, Ana Ortiz-Atienza<sup>1</sup> , Rosa Micol-Ponce<sup>1</sup> , Trinidad Angosto<sup>1</sup> , Juan Capel<sup>1</sup> , Vicente Moreno<sup>2</sup> , Fernando J. Yuste-Lisbona<sup>1</sup>  and Rafael Lozano<sup>1</sup> 

<sup>1</sup>Centro de Investigación en Biotecnología Agroalimentaria (CIAIMBITAL), Universidad de Almería, Almería 04120, Spain; <sup>2</sup>Instituto de Biología Molecular y Celular de Plantas (UPV-CSIC), Universidad Politécnica de Valencia, 46022 Valencia, Spain

## Summary

Author for correspondence:  
Rafael Lozano  
Email: rlozano@ual.es

Received: 19 November 2021  
Accepted: 3 February 2022

New Phytologist (2022) 234: 1059–1074  
doi: 10.1111/nph.18034

**Key words:** carpel development, *CRABS CLAW* (*CRC*), floral meristem determinacy, fruit formation, incomplete penetrance, tomato (*Solanum lycopersicum*), variable expressivity, *WUSCHEL* (*WUS*).

- *CRABS CLAW* (*CRC*) orthologues play a crucial role in floral meristem (FM) determinacy and gynoecium formation across angiosperms, the key developmental processes for ensuring successful plant reproduction and crop production. However, the mechanisms behind *CRC* mediated FM termination are far from fully understood.
- Here, we addressed the functional characterization of tomato (*Solanum lycopersicum*) paralogous *CRC* genes. Using mapping-by-sequencing, RNA interference and CRISPR/Cas9 techniques, expression analyses, protein–protein interaction assays and Arabidopsis complementation experiments, we examined their potential roles in FM determinacy and carpel formation.
- We revealed that the incomplete penetrance and variable expressivity of the indeterminate carpel-inside-carpel phenotype observed in *fruit iterative growth* (*fig*) mutant plants are due to the lack of function of the *S. lycopersicum* *CRC* homologue *SICRCa*. Furthermore, a detailed functional analysis of tomato *CRC* paralogues, *SICRCa* and *SICRCb*, allowed us to propose that they operate as positive regulators of FM determinacy by acting in a compensatory and partially redundant manner to safeguard the proper formation of flowers and fruits.
- Our results uncover for the first time the physical interaction of putative *CRC* orthologues with members of the chromatin remodelling complex that epigenetically represses *WUSCHEL* expression through histone deacetylation to ensure the proper termination of floral stem cell activity.

## Introduction

From their outermost to the innermost whorls, flowers typically consist of sepals, petals, stamens and carpels that are generated from a pool of stem cells located in floral meristems (FM) (Krizek & Fletcher, 2005). Once a set number of floral organs have been initiated, stem cell activity is arrested, and the FM is thereby determined to form the gynoecium. The precise timing of this developmental event, also referred to as floral determinacy, is a pivotal process that establishes the number of floral organs arising from the FM (Sun & Ito, 2015).

In Arabidopsis, the homeodomain transcription factor *WUSCHEL* (*WUS*) is responsible for maintaining stem cell activity in the FM, while the MADS-box transcription factor *AGAMOUS* (*AG*) regulates the timing of FM termination by repressing *WUS* expression (Liu *et al.*, 2011). *AG* turns off the stem cell maintenance programme involving transcriptional repression of *WUS* by different pathways: directly by a

mechanism that implicates chromatin remodelling and the recruitment of the Polycomb group (PcG) protein TERMINAL FLOWER2/LIKE HETEROCHROMATIN PROTEIN1 (TFL2/LHP1) at the *WUS* locus (Guo *et al.*, 2018), and indirectly through the transcriptional induction of the two key targets, *KNUCKLES* (*KNU*) and *CRABS CLAW* (*CRC*). *KNU* and *CRC* act through independent pathways to synergistically regulate *WUS* repression, thus ensuring FM determination (Sun *et al.*, 2009, 2014, 2019; Yamaguchi *et al.*, 2017, 2018). *KNU* encodes a C2H2 zinc-finger protein whose expression is activated by *AG*, a process that requires a time-delay induction regulated by epigenetic modification of histones at the *KNU* locus (Sun *et al.*, 2014). Once induced, *KNU* binds to the *WUS* promoter, which causes the eviction of *SPLAYED*, a chromatin remodelling factor required for *WUS* activation, and mediates the subsequent deposition of H3K27me3 for stable Polycomb-mediated repression *WUS* (Kwon *et al.*, 2005; Sun *et al.*, 2019). Furthermore, *AG* also positively regulates *MINI ZINC FINGER2* (*MIF2*)

expression during flower development, which acts as an adaptor protein to form a transcriptional repressor complex together with KNU, the transcriptional corepressor TOPLESS (TPL) and the chromatin remodelling protein HISTONE DEACETYLASE19 (HDA19). Within this complex, MIF2 binds to the *WUS* locus, leading to the epigenetic repression of *WUS* expression through histone deacetylation (Bollier *et al.*, 2018). Concurrently, the YABBY transcription factor CRC, a direct target of AG, mediates auxin homeostasis and establishes auxin maxima during carpel primordium initiation by repressing *TORNADO2* (*TRN2*) and up-regulating the auxin synthesis gene *YUCCA4* (*YUC4*). The proper auxin maxima mediated by *CRC* contribute to the termination of FM cell proliferation through *WUS* repression and trigger the subsequent gynoecium formation (Yamaguchi *et al.*, 2017, 2018).

In tomato (*Solanum lycopersicum*), the molecular mechanisms underlying *SIWUS* transcriptional regulation during floral development are of agronomic interest, as mutations leading to a spatial and temporal expansion of its expression domains result in flowers with extra carpels, which give rise to larger multilocular fruits (Rodríguez-Leal *et al.*, 2017; Yuste-lisbona *et al.*, 2020). Likewise, alterations in FM determinacy potentially lead to a reiterative carpel formation pattern resulting in indeterminate fruits, which makes a developmental process closely related to fruit shape and size, the two quality attributes that influence consumer's acceptance and post-harvest handling. Recently, Bollier *et al.* (2018) have proposed a conserved molecular mechanism regulating FM determinacy in Arabidopsis and tomato. Thus, the interaction between tomato MIF2 and KNU orthologues, INHIBITOR OF MERISTEM ACTIVITY (SIIMA) and SIKNU, allows for the recruitment of tomato TPL and HDA19 orthologues, SITPL1 and SIHDA1, to form a transcriptional repressor complex at the *SIWUS* locus. Here, we provide insights into the genetic and molecular mechanisms involved in FM determinacy and carpel development. Our results revealed that the loss of carpel determinacy observed in the *fruit iterative growth* (*fig*) mutants is due to the lack of function of the *S. lycopersicum* *CRC* homologue *SICRCa*. Furthermore, functional analysis of tomato *CRC* paralogues, *SICRCa* and *SICRCb*, allowed us to uncover for the first time the role of *CRC* orthologues as members of the molecular network that epigenetically represses *WUS* through histone deacetylation to ensure the proper termination of floral stem cell activity.

## Materials and Methods

### Plant material and growth conditions

The *fig* mutant was identified from a T-DNA insertional mutant collection generated in the genetic background cultivar P73 (Pérez-Martín *et al.*, 2017). However, molecular analysis showed that the *fig* mutation was not associated with a T-DNA insertion (Supporting Information Fig. S2, see later). For mapping-by-sequencing, an F<sub>2</sub> mapping population was generated by crossing a *fig* mutant to wild tomato *Solanum pimpinellifolium* (accession no. LA1589) and self-fertilizing the F<sub>1</sub> plants. *Arabidopsis*

*thaliana* plants used for this study, including mutant and transgenic plants, were in the ecotype Landsberg *erecta* (*Ler*) genetic background (kindly provided by Prof. M. R. Ponce, Miguel Hernández University, Elche, Spain). The seeds of the *crabs claw-1* (*crc-1*; CS3814; N3814) mutant (Alvarez & Smyth, 1999) were initially obtained from the Nottingham Arabidopsis Stock Center (NASC, Nottingham, UK) and propagated at our laboratory for further analysis. Tomato and Arabidopsis growth conditions are given in Methods S1.

### Phenotypic characterization of tomato flowers and fruits

The number of floral organs was evaluated in at least 60 tomato (*Solanum lycopersicum* L.) flowers at anthesis stage showing wild-type (WT)-like, weak and severe phenotypes. A minimum of 60 mature fruits were collected and used to calculate the average fruit weight (g), width (mm), length (mm) and number of locules per phenotype.

Optical microscopy and scanning electron microscopy (SEM) analyses were performed as described in Lozano *et al.* (1998). Sample processing and visualization techniques are described in Methods S2.

### Whole-genome sequencing and candidate gene identification

Mapping-by-sequencing was performed as described previously (Yuste-Lisbona *et al.*, 2021). The F<sub>2</sub> mapping population was generated by crossing *fig* to wild tomato *S. pimpinellifolium* (accession no. LA1589) and self-fertilizing the F<sub>1</sub> plants. Two DNA pools of contrasting phenotype were sequenced using Illumina 100-bp paired-end reads. The resulting reads were deposited in the Sequence Read Archive (SRA) database (<http://www.ncbi.nlm.nih.gov/sra>) under BioProject accession no. PRJNA685617. Reads were aligned to the tomato genome reference sequence v.4.0 (ITAG4.0) using BOWTIE2 (Langmead & Salzberg, 2012). The allele frequency ratio for biallelic variants was calculated as nonreference allele counts/total allele counts using a custom script in R v.4.0.1 (R Development Core Team, 2020). The average allele frequencies were plotted along each chromosome using a sliding window and step size of 1000 and 100 variants, respectively. Once the candidate gene was determined, *SICRCa* locus was genotyped using the *SICRCa-Fg* and *SICRCa-Rg* primers in the F<sub>2</sub> population (primer sequences in Table S1).

### Quantitative real-time PCR

The quantitative real-time PCR (qRT-PCR) analysis was carried out using three biological and two technical replicates. One microgram of RNA was used for cDNA synthesis with a ML-MLV reverse transcriptase (Invitrogen, San Diego, CA, USA) with a mixture of random hexamer and oligo-(dT)<sub>18</sub> primers. Specific primer pairs (sequences listed in Table S2) were used in each qRT-PCR with the SYBR Green PCR Master Mix Kit (Applied Biosystems, Foster City, CA, USA) on the 7300 Real-Time PCR System (Applied Biosystems). The housekeeping

gene *Ubiquitin3* (*Solyc01g056940*) was used as a control. Gene expression was quantified using the  $\Delta\Delta C_t$  calculation method (Winer *et al.*, 1999).

### Generation of tomato transgenic lines

To generate the RNA interference (RNAi) *SICRCa* construct, a 118-bp fragment of the *Solyc01g0104120* first exon was amplified using the *SICRCa*-Fi and *SICRCa*-Ri primers and cloned in sense and antisense orientation into the pKannibal vector (Wesley *et al.*, 2001). The modified pKannibal vector was digested with *NotI*, and the resulting restriction fragment was cloned into the pART27 vector (Gleave, 1992). *SICRCa* and *SICRCb* CRISPR/Cas9 lines were obtained following the protocol described by Vazquez-Vilar *et al.* (2016). The BREAKING-CAS software (Oliveros *et al.*, 2016) was used to design the single-guide RNA (sgRNA) target sequences within the coding region of *SICRCa* (GTA TCCAACAACCTTCTTGCA) and *SICRCb* (GTATCCATTAG CCTCTTGTA). Primers used in the generation of RNAi and CRISPR/Cas9 constructs are shown in Table S1. Genetic transformation experiments were developed as described in Ellul *et al.* (2003), using *Agrobacterium tumefaciens* LBA4404 strain. *CR-slcrc:a:slcr:b* double-mutant plants were generated using standard crossing between single *slcr:b* and *slcr:a* T<sub>0</sub> CRISPR null mutants and were confirmed by genotyping from F<sub>1</sub> progeny plants.

### In situ hybridization analysis

Tissue preparation, sectioning and transcript detection for *in situ* hybridization experiments were carried out as described in Lozano *et al.* (1998). *SICRCa* (*Solyc01g0104120*), *SICRCb* (*Solyc05g012050*) and *SIWUS* (*Solyc02g083950*) probes were synthesized using cDNA as a template by using the primers *SICRCa*-Fz/*SICRCa*-Rz, *SICRCb*-Fz/*SICRCb*-Rz and *SIWUS*-Fz/*SIWUS*-Rz (sequences are reported in Table S2), respectively. The antisense probe was synthesized using the DIG RNA labelling mix (Roche Applied Science, Indianapolis, IN, USA). As a negative control, sense RNA probes were synthesized and hybridized to sections of tomato floral buds.

### RNA sequencing

Three biological replicates per genotype were sequenced, each with at least 30 floral buds at developmental stages 0–6. RNA-sequencing (RNA-seq) libraries were prepared from total RNA according to the Illumina TruSeq RNA protocol and sequenced using Illumina 150-bp paired-end reads. The resulting reads were deposited in the SRA database under BioProject accession no. PRJNA686085. Reads were aligned to the tomato genome reference sequence v.4.0 (ITAG4.0) using TOPHAT v.2.0.6 (Kim *et al.*, 2013). The raw number of reads per transcript was counted using the Bioconductor packages GenomicFeatures and GenomicAlignments (Lawrence *et al.*, 2013). Differentially expressed genes (DEGs) were determined using the Wald test in the DESeq2 package (Love *et al.*, 2014). Genes with a false discovery rate (FDR)-adjusted *P*-value < 0.05 were defined as significantly

deregulated. Gene Ontology (GO) term enrichment analysis of DEGs was performed using AGRIGO v.2.0 (Tian *et al.*, 2017).

### Molecular complementation of the Arabidopsis *crc-1* mutant

The *crc-1* mutant (Alvarez & Smyth, 1999) in the ecotype Landsberg *erecta* (*Ler*) genetic background was obtained from the Nottingham Arabidopsis Stock Center (NASC ID: N3814). *crc-1* was complemented with two different constructs, each carrying a 3860-bp fragment from upstream of the Arabidopsis *CRC* start codon representing its promoter region (*pCRC*), fused to the coding sequences of either the tomato *SICRCa* (*pCRC::SICRCa*) or *SICRCb* (*pCRC::SICRCb*) genes. PCR products were purified and cloned into the pGEM-T vector (Promega). *pCRC* and each gene coding fragment were linked by a double digestion with *XhoI* and a specific restriction enzyme, which cuts within the pGEM-T polylinker (*AatII* or *SacI* depending on the *pCRC* and coding sequence orientation in the pGEM-T) and subsequent ligation conducted by T4 DNA ligase. The complete sequences of the *pCRC* fused to the corresponding gene coding sequence were obtained by amplifying with *pCRC*-Fac/*SICRCa*-Rac or *pCRC*-Fac/*SICRCb*-Rac primers, then cloned into the pENTR/D-TOPO vector (Invitrogen), and finally subcloned into the Gateway vector pGWB401 (Nakagawa *et al.*, 2007). The primers used in the generation of constructs are shown in Table S3. Plasmids were transformed into an *A. tumefaciens* C58C1 strain. The plants of *Ler* and *crc-1* were transformed by the floral dip method described by Clough & Bent (1998). At least 30 flowers and siliques from *Ler*, *crc-1* and T<sub>1</sub> transgenic plants, resulting from the transformation of *Ler* and *crc-1* plants with either *pCRC::SICRCa* or *pCRC::SICRCb* constructs, were evaluated under a Leica DMS1000 digital microscope.

### Sequence alignment and microsynteny analysis

The amino acid sequences of *SICRCa* (XP\_004228849), *SICRCb* (XP\_004239032) and *CRC* (NP\_177078) were downloaded from the GenBank database (<http://www.ncbi.nlm.nih.gov>) and pairwise aligned using BLASTP (<https://blast.ncbi.nlm.nih.gov/Blast.cgi>). Microsynteny between the genomic regions harbouring the Arabidopsis *CRC* gene and either the tomato *SICRCa* or *SICRCb* genes was analysed with the GEvo tool (<https://genomeevolution.org/coge/GEvo.pl>).

### Subcellular localization and bimolecular fluorescence complementation assays

*SICRCa* and *SICRCb* subcellular localizations were assessed by fusing each protein to the green fluorescent protein (GFP). Thus, coding sequences for *SICRCa* and *SICRCb* proteins were cloned into the pENTR/D-TOPO vector and recombined into the Gateway vector pGWB6 (Nakagawa *et al.*, 2007) to integrate GFP at the N-terminus of the proteins of interest. To test for bimolecular fluorescence complementation (BiFC)-based protein–protein interaction, coding sequences of *SICRCa*, *SICRCb*,

SIKNU, SIIMA, SIHDA1 and SITPL1 proteins were cloned into the pENTR/D-TOPO vector and subcloned into the Gateway vectors containing the N- or C-terminal fragments of the yellow fluorescent protein (YFP) (pYFN43 and pYFC43 vectors, respectively). The  $\beta$ -glucuronidase (GUS) enzyme, encoded by the *uidA* gene from *Escherichia coli*, fused to N- or C-terminal fragments of YFP was used as negative control. Constructs were transformed in *A. tumefaciens* GV3101 strain and infiltrated into *Nicotiana benthamiana* leaves from 2- to 3-wk-old plants. Plants were kept in long-day (16 h : 8 h, light : dark) conditions at 22°C. Samples were observed 3 d post-infiltration using a Nikon Eclipse Ti confocal microscope. The sequences of primers used for subcellular localization and BiFC assays are shown in Table S4.

### Co-immunoprecipitation assays

The leaves of *N. benthamiana* were transiently co-transfected with *A. tumefaciens* GV3101 strain cultures expressing either GFP-tagged SICRCa (SICRCa<sup>GFP</sup>) or SICRCb (SICRCb<sup>GFP</sup>) and the different hemagglutinin (HA)-tagged members of the chromatin remodelling complex (SIKUN<sup>HA</sup>, SIIMA<sup>HA</sup>, SIHDA1<sup>HA</sup> or SITPL1<sup>HA</sup>). Likewise, the SICRCb<sup>GFP</sup> was co-transfected with HA-tagged SICRCa (SICRCa<sup>HA</sup>). For this purpose, pENTR/D-TOPO vectors containing full open reading frame sequences of the recombinant fusion proteins of interest were recombined into the Gateway vectors pGWB6 and pGWB15 (Nakagawa *et al.*, 2007), containing GFP and HA tags, respectively. These vectors were co-infiltrated in *N. benthamiana* leaves from 2- to 3-wk-old plants. Plants were kept under long-day (16 h : 8 h, light : dark) conditions at 22°C. Subsequent protein extraction was performed from the leaves harvested 2 d after infiltration. Plant material was ground in liquid nitrogen and homogenized in protein extraction buffer (25 mM Tris-HCl, pH 7.4, 75 mM NaCl, 0.5% Nonidet P-40, 0.05% sodium deoxycholate, 10 mM  $\beta$ -mercaptoethanol, 1 mM PMSF and cOmplete, EDTA-free Protease Inhibitor Cocktail (Roche Applied Science)). Protein extracts were centrifuged twice at 14 000 g for 10 min at 4°C. After cell lysis, GFP-tagged proteins were magnetically labelled and subsequently isolated using a  $\mu$ MACS Isolation kit (Miltenyi Biotec, Bergisch Gladbach, Germany). The resulting samples were analysed by SDS-PAGE and immunoblotted using anti-GFP-HPR (Miltenyi Biotec) and anti-HA-peroxidase (Roche Applied Science) antibodies.

## Results

### *fig* mutation impairs carpel determinacy

The *fruit iterative growth* (*fig*) mutant was isolated from the screening of a collection of T<sub>1</sub>-segregating T-DNA lines generated from the tomato cultivar P73 (Pérez-Martín *et al.*, 2017). Vegetative development of *fig* plants was indistinguishable from that of WT ones, whereas significant differences were observed during flower and fruit development (Fig. 1a–c; Table S5). *fig* flowers developed an elevated number of organs in all whorls, this

increase being more evident in carpels. Thus, carpel formation occurs repeatedly in the gynoeceum of *fig* flowers leading to anomalous fruits, that show secondary fruit structures growing in an indeterminate way that appeared from the inside of the principal fruit (Fig. 1a–c; Table S5).

The observed phenotypic segregation (39 WT: 15 *fig*) was consistent with a monogenic recessive inheritance of the *fig* mutation ( $\chi^2 = 0.22$ ;  $P = 0.64$ ). However, the *fig* phenotype showed incomplete penetrance and variable expressivity, as a gradation of phenotypes was displayed within the same mutant plant, even within the same inflorescence. Therefore, variable flower and fruit phenotypes were observed in *fig* plants, which were classified as WT-like (indistinguishable from WT), weak and severe indeterminate phenotypes (Figs 1a–c, S1), the average production of fruits with severe phenotype being close to 50% per *fig* plant (Fig. 1d).

A SEM study in developing flowers revealed that the first visible anomalies could be detected at floral stage 5 (Brukhin *et al.*, 2003). At this stage, carpels emerge, and ovary cavities become visible showing abnormal carpel structures in both weak and severe *fig* flowers (Fig. 1f,g). At stage 8, WT pistils are formed by 3–4 carpels (Fig. 1e), whereas an increased number of carpels are observed in *fig* flowers resulting in incomplete fused pistils (Figs 1f,g, S1). Histological sections of flowers at anthesis day showed that *fig* pistils have shorter and thicker styles and are composed of numerous carpels that grow one inside another, which strongly suggests that *fig* mutation affects carpel determinacy. These differences were more accentuated in severe *fig* flowers (Fig. 1c,g), producing ovaries 3-fold bigger than the WT ones at anthesis day stage (Fig. 1a,e). As a result of this variable range of *fig* flower phenotypes, we observed both weak *fig* fruits producing secondary fruit structures only visible inside the fruit (Fig. 1b), and severe *fig* fruits where these secondary fruit structures emerged from inside and were visible outside the fruit (Figs 1c, S1). Despite such abnormalities and although more extreme *fig* fruits produced fewer seeds, *fig* mutants gave rise to viable seeds.

Molecular analyses revealed that the *fig* mutation was not associated with a T-DNA insertion (Fig. S2), suggesting that a somaclonal variation produced during the *in vitro* culture process is responsible for the mutant phenotype. To identify the causative mutation underlying the *fig* phenotype, we performed a mapping-by-sequencing strategy using an F<sub>2</sub> population derived from crossing *fig* to the wild tomato *S. pimpinellifolium* (accession no. LA1589). A total of 783 F<sub>2</sub> plants were scored for ovary and fruit development, from which 212 plants produced fused carpels and indeterminate fruits. The phenotypic segregation observed in this F<sub>2</sub> progeny (571 WT: 212 *fig*) was consistent with a monogenic recessive inheritance of the *fig* mutation ( $\chi^2 = 1.80$ ,  $P = 0.18$ ). We then conducted genome sequencing of two DNA pools containing 50 WT and 25 *fig* F<sub>2</sub> plants with the most strongly indeterminate phenotype. Genome-wide analysis of the allele frequencies revealed a region encompassing the centromere of chromosome 1 (2.4–70 Mb) with a strong bias towards tomato reference alleles (Fig. 2a). Variant analysis in this candidate region identified three SNPs mapping at the fourth intron of the *Solyc01g010240* gene, which also showed a marked decrease in the sequence coverage of the mutant pool compared with other

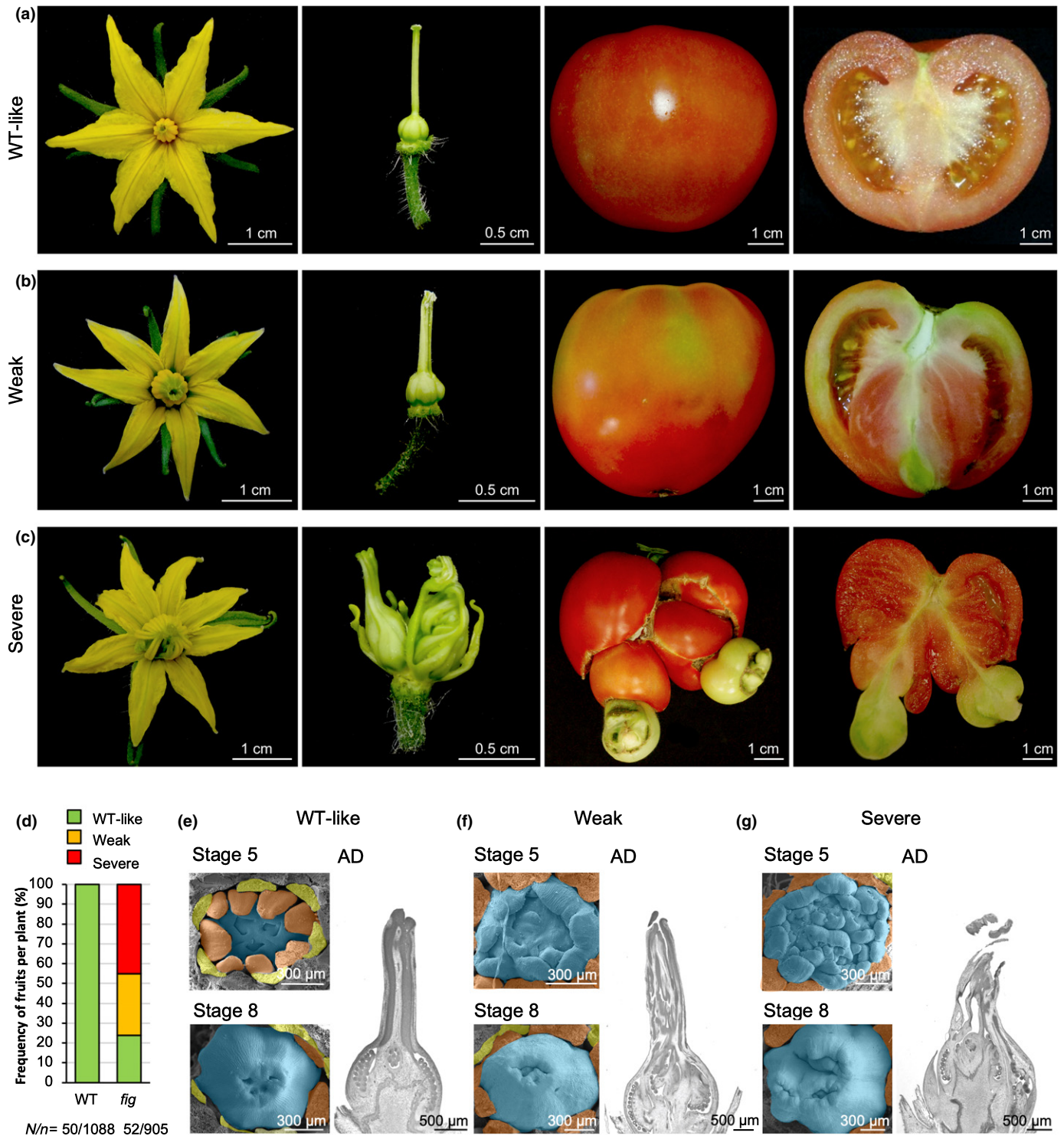


**Fig. 1** Phenotypic characterization of the tomato (*Solanum lycopersicum*) *fig* mutant. (a–c) Representative *fig* flowers, pistils, closed fruits and longitudinal open fruits (from left to right) showing WT-like (identical to wild-type, WT) (a), weak (b) and severe (c) phenotypes. (d) Percentage of different types of fruits (WT-like, weak or severe) produced by WT (cv P73) and *fig* plants. *N*, number of plants evaluated; *n*, number of fruits harvested. (e–g) Scanning electron microscopy images of flowers at stages 5 and 8 of floral development, and histological sections of flowers at anthesis day (AD) stage exhibiting WT-like (e), weak (f) and severe (g) phenotypes. Sepals were removed in samples at stage 5, whereas only the carpels were maintained in developing flowers at stage 8. Petals are coloured in yellow, stamens in orange and carpels in blue.

coding and noncoding regions of this gene. PCR analyses with primers flanking the region containing these SNPs in WT and *fig* plants showed that the PCR product from *fig* genomic DNA was

larger than expected. Sequence analysis verified that a DNA fragment of 367 bp was inserted at position 5053 687 on the chromosome 1 of the mutant genome (Assembly SL4.0), interrupting

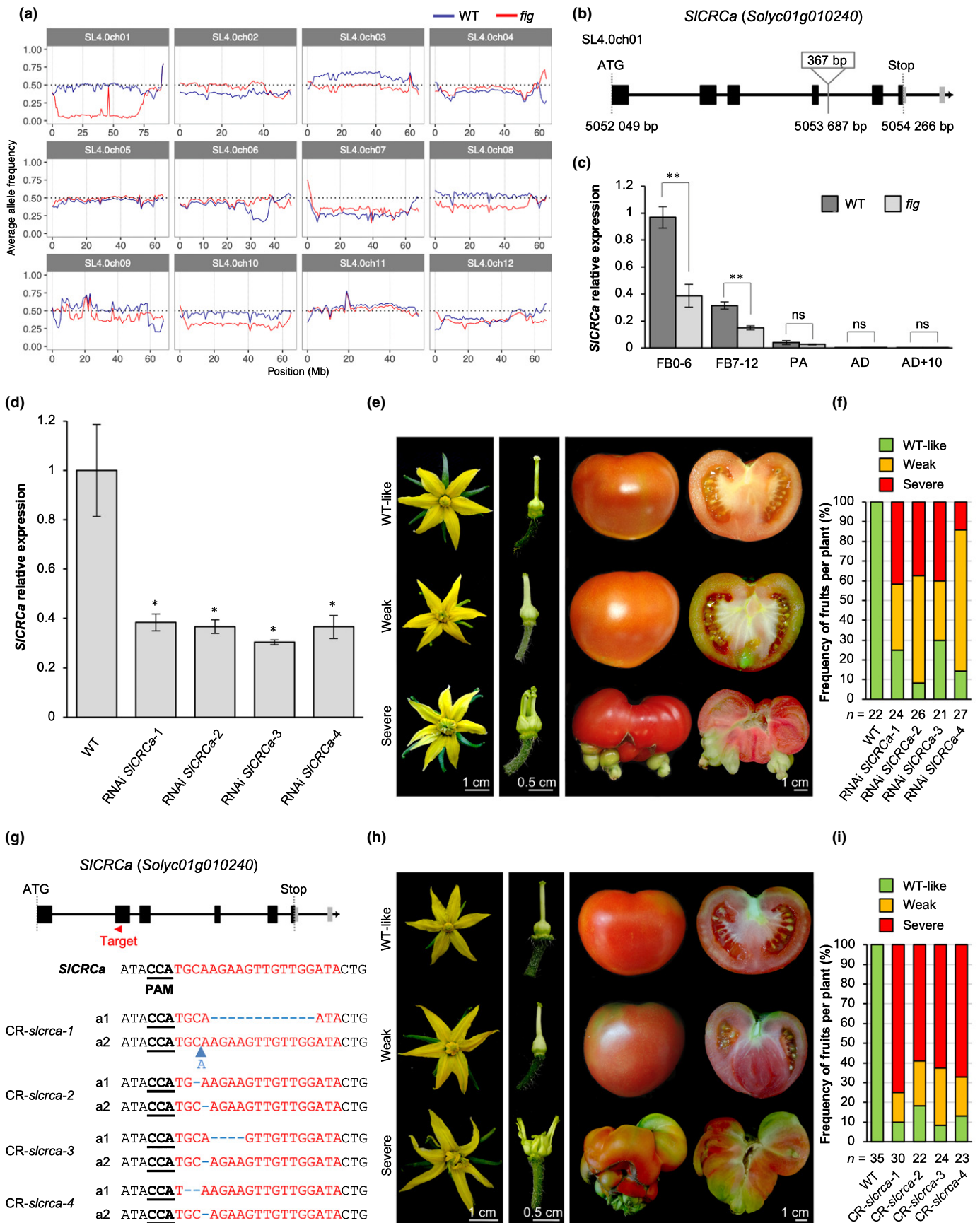


**Fig. 2** Tomato *FIG* gene encodes a homologue of the Arabidopsis *CRC* gene. (a) Distribution of the average allele frequency of wild-type (WT; blue line) and *fig* (red line) pools grouped by chromosomes. (b) Schematic representation of the *SICRCa* gene (introns are represented by black lines, and coding and UTRs are in black and grey boxes, respectively) and the 367-bp sequence inserted at the fourth intron in *fig* mutants. (c) Relative expression of *SICRCa* in WT and *fig* flowers at different stages of floral development. FB0–6, floral buds from stages 0 to 6; FB7–12, floral buds from stages 7 to 12; PA, flowers at pre-anthesis stage; AD, flowers at anthesis stage; AD+10, flowers 10 d after anthesis stage. (d) *SICRCa* transcripts quantification of flowers at stage FB0–6 from RNAi *SICRCa* and WT lines. (e) Representative RNAi *SICRCa* flowers, pistils and fruits displaying WT-like, weak and severe mutant phenotypes. (f) Percentage of different types of fruits harvested from WT and T<sub>0</sub> RNAi *SICRCa* plants. (g) CRISPR/Cas9-*slcrca* (CR-*slcrca*) alleles identified by cloning and sequencing PCR products from the *SICRCa*-targeted region from four T<sub>0</sub> CRISPR/Cas9 plants. Black bold and underlined letters indicate protospacer adjacent motif (PAM) sequences, blue dashed lines show InDel mutations, and blue letter and arrow indicate an insertion sequence. (h) Representative CR-*slcrca* flowers, pistils and fruits exhibiting WT-like, weak and severe phenotypes. (i) Percentage of different types of fruits harvested from WT and T<sub>0</sub> CR-*slcrca* plants. In (f, i), *n* value indicates the number of fruits harvested per plant. In (c, d), data are means ± SD of three biological and two technical replicates. A two-tailed, two-sample Student *t*-test was performed, and significant differences are represented by asterisks: \*, *P* < 0.01; \*\*, *P* < 0.001; ns, no statistically significant differences.

the intron sequence between the *Solyc01g010240* exons 4 and 5 (Fig. 2b). This insertion shares a sequence identity of 86% with the long terminal repeat (LTR) copy placed between 6336 872 and 6337 201 positions on the chromosome 10, which may have acted as a transposable element. Co-segregation analysis performed in the F<sub>2</sub> population showed that all 212 *fig* mutant plants were homozygous for the 367-bp LTR insertion, whereas 393 and 178 phenotypically WT plants were hemizygous or lacked the LTR insertion, respectively, indicating that the *fig* phenotype co-segregated with the LTR insertion at the *Solyc01g010240* gene.

Notwithstanding that the 367-bp insertion occurs at a noncoding region, we considered the *Solyc01g010240* gene as a strong candidate to be responsible for the *fig* phenotype, since it is the homologue of the Arabidopsis *CRC* gene, *SICRCa*, a putative transcription factor of the YABBY gene family previously described as involved in carpel and nectary development and FM determination (Alvarez & Smyth, 1999; Bowman & Smyth, 1999). To determine the effects of the LTR insertion on *SICRCa* expression, cDNA cloning and qRT-PCR analyses were performed. The sequences of WT and mutant cDNAs were identical, but *SICRCa* expression was significantly reduced in floral buds of the *fig* mutant, at stages 0–6 and 7–12 (Fig. 2c). Thus, the 367-bp insertion reduced *SICRCa* transcript level to > 2-fold but still allowed the production of WT *SICRCa* mRNA, suggesting that the fourth *SICRCa* intron may contain a transcriptional regulatory element critical for the maintenance of the *SICRCa* spatio-temporal expression pattern.

To corroborate whether the lack of *SICRCa* function is responsible for the *fig* phenotype, we generated RNAi-mediated knock-down lines with reduced levels of *SICRCa* transcripts. Four independent first-generation (T<sub>0</sub>) RNAi *SICRCa* diploid lines were evaluated, which showed > 2-fold decrease in *SICRCa* expression in floral buds at stages 0–6 (Fig. 2d). As happened with the *fig* mutation, RNAi *SICRCa* lines displayed a variable range of flower phenotypes, resulting in the development of fruits with WT-like, weak and severe indeterminate phenotypes (Fig. 2e,f). Furthermore, we engineered knockout mutations using the CRISPR/Cas9 system with a sgRNA targeting the second exon of *SICRCa* (Fig. 2g). We assessed four independent T<sub>0</sub> diploid lines (CR-*slcrca*) that were biallelic for edited knockout alleles (Fig. 2g). CR-*slcrca* lines developed flowers and fruits, which undoubtedly resembled the phenotype observed in *fig*

mutants, and they also produced a wide diversity of flower and indeterminate fruit phenotypes, most of them classified as severe (Fig. 2f,h). Therefore, although there were differences in the percentages of fruits with the severe mutant phenotype, both knock-down (RNAi) and knockout (CRISPR/Cas9) alleles resulted in the similar phenotypes with incomplete penetrance and variable expressivity, indicating that any deficiency in *SICRCa* function might lead to a loss of FM determinacy.

#### *SICRCa* expression is restricted to carpels

As expected from the *fig* phenotype, *SICRCa* expression was mainly restricted to flowers at early developmental stages. The higher *SICRCa* expression was found in floral buds at stages 0–6 (Fig. 3a). RNA *in situ* hybridization analysis revealed that *SICRCa* transcripts were accumulated specifically in carpel primordia when they were initiated at floral stage 3 (Fig. 3b), and persisted in these primordia at floral stage 6, when carpels were growing up and the primordium of placenta emerged (Fig. 3c). At floral stage 8, *SICRCa* expression was located at the adaxial surface on the base of the ovary walls, as well as in the most distal cells of the developing gynoecium, which would produce the style and the stigma (Fig. 3d). However, *SICRCa* mRNA was not detected in the ovary walls at floral stage 9, and its expression remained in the distal part of the gynoecium (Fig. 3e). At later stages of floral development, there was no evidence of detectable *SICRCa* transcripts.

RNA-seq was next performed on WT and *fig* floral buds at developmental stages 0–6 to gain insight into the functional role of *SICRCa*. This analysis identified 2115 DEGs in *fig* as compared to WT, of which 978 were up-regulated and 1137 were down-regulated (Table S6). To investigate the functions of DEGs, we applied a GO enrichment analysis, which revealed 29 and 36 over-represented GO terms for up- and down-regulated DEGs, respectively (Table S7). For biological process, GO terms belonging to response to stimulus (GO: 0050896) were enriched in both groups of DEGs. However, biological processes related to reproduction (GO: 0000003), reproductive process (GO: 0022414), developmental process involved in reproduction (GO: 0003006), reproductive structure development (GO: 0048608) and flower development (GO: 0009908) were enriched among up-regulated DEGs. Regarding molecular function, GO terms involved in protein binding (GO: 0005515) were enriched in both up- and down-regulated DEGs. In addition, transporter activity

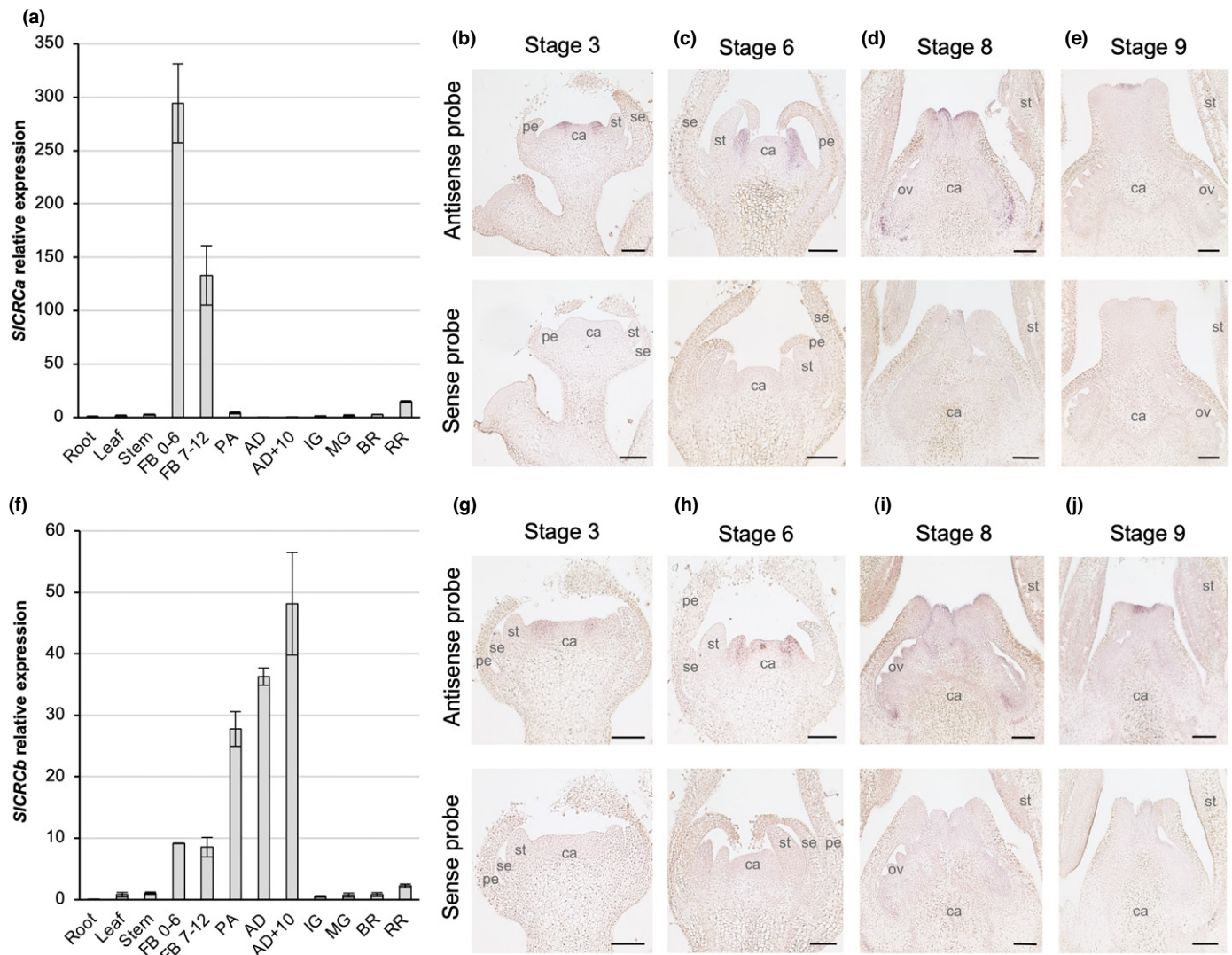


**Fig. 3** Dynamic expression of tomato *SICRCa* and *SICRCb* genes. (a) Relative expression of *SICRCa* determined by qRT-PCR in different developmental tissues and stages of wild-type (WT) flowers. (b–e) *In situ* mRNA hybridization of *SICRCa* using antisense or sense probes in histological sections of WT flowers at different developmental stages: stage 3 (b), stage 6 (c), stage 8 (d) and stage 9 (e). (f) Relative expression of *SICRCb* determined by qRT-PCR in different developmental tissues and stages of WT flowers. (g–j) *In situ* mRNA hybridization of *SICRCb* using antisense or sense probes in histological sections of WT flowers at different developmental stages: stage 3 (g), stage 6 (h), stage 8 (i) and stage 9 (j). In (a, f), data are means  $\pm$  SD of three biological and two technical replicates. FB0-6, floral buds from stages 0 to 6; FB7-12, floral buds from stages 7 to 12; PA, flowers at pre-anthesis stage; AD, flowers at anthesis stages; AD+10, flowers 10 d after anthesis stage; IG, immature green fruit; MG, mature green fruit; BR, breaker fruit; and RR, mature red fruit. Bars, 100  $\mu$ m; the floral organ primordia of sepal (se), petal (pe), stamen (st) and carpel (ca), as well as ovules (ov) in the carpel cavities, are indicated.

(GO:0005215) and transcription factor activity of sequence-specific DNA binding (GO:0003700) terms were enriched in up-regulated DEGs (Table S7; Fig. S3).

Among the up-regulated DEGs annotated with the reproductive structure development (GO:0003700) and flower development (GO:0009908) terms, we found the homologues of the Arabidopsis PIN-FORMED auxin efflux carrier (Soly-c03g118740, Soly-c04g007690 and Soly-c05g008060) and the AUXIN RESPONSE FACTOR transcription factor (Soly-c09g007810 and Soly-c12g042070) families, as well as the homologues of the floral homeotic genes *APETALA2* (Soly-c02g064960), *APETALA3* (Soly-c04g081000), *FRUITFULL* (Soly-c03g114830) and *SEPALLATA4* (Soly-c03g114840), the

latter of which is also involved in the determination of FM (Ditta *et al.*, 2004). Within this group of genes, we also found the homologue of the Arabidopsis *HECATE3* (Soly-c11g005780), whose overexpression causes the production of ectopic stigmatic tissue (Gremski *et al.*, 2007). Remarkably, a second homologue of the Arabidopsis *CRC* gene (*SICRCb*, Soly-c05g012050) was moreover included in this group of up-regulated DEGs.

#### Knockout mutations in *SICRCb* mimic *fig* mutant phenotype

While the Arabidopsis genome carries one copy of the *CRC* gene, an ancestral duplication in Solanaceae generated two paralogues,



*CRCa* and *CRCb*, whose retention across Solanaceae genomes suggests functional relevance (Phukela *et al.*, 2020). Sequence analysis of the Arabidopsis CRC (181 aa) and the tomato SICRCa (173 aa) and SICRCb (160 aa) amino acid sequences displayed that CRC has an identity of 64 and 68% to SICRCa and SICRCb, respectively; while SICRCa shows 73% identity to SICRCb. Microsynteny study between genomic blocks harbouring *CRC* genes in Arabidopsis and tomato showed that the Arabidopsis genomic region containing *CRC* was more closely related to that in tomato, which bears *SICRCb* rather than *SICRCa* (Fig. S4). To gain further insight into the role of *SICRCb*, we examined its spatio-temporal expression. As with *SICRCa*, a specific expression in reproductive tissues was observed for *SICRCb* (Fig. 3a,f), although *SICRCb* transcripts were detected throughout all floral development stages, from floral buds at developmental stages 0–6 to flowers at 10 d post-anthesis (Fig. 3f), whereas *SICRCa* expression was mainly detected at first stages of floral bud development (Fig. 3a). Even though *SICRCa* and *SICRCb* showed differential temporal expression patterns, *in situ* hybridization studies in developing flowers revealed that *SICRCb* shows an identical spatial expression profile to *SICRCa*. Thus, *SICRCb* transcript accumulation was first localized at floral stage 3 in carpel primordia (Fig. 3g), where it continued until floral stage 6 (Fig. 3h). As the development progressed to floral stage 8, *SICRCb* expression was detected in the ovary walls and the distal regions of the developing gynoecium (Fig. 3i), where its expression remained restricted at floral stage 9 (Fig. 3j).

The incomplete penetrance and variable expressivity of mutations at the *SICRCa* locus, as well as the overlapping *SICRCa* and *SICRCb* spatial expression patterns at the initiation of gynoecium development, led to a hypothesis that a partial redundancy of tomato *CRC* paralogues may exist. To test this hypothesis, we generated knockout mutations using CRISPR/Cas9 system with a sgRNA targeting the second exon of *SICRCb* (Fig. 4a). We evaluated four independent T<sub>0</sub> diploid lines (CR-*slcrb*) homozygous or biallelic for edited knockout alleles (Fig. 4a). CR-*slcrb* lines produced flowers with ovaries composed of numerous carpels growing inside one another, which led to anomalous fruits similar to those observed in *fig* mutants, RNAi *SICRCa* and CR-*slerca* lines (Fig. 4b). CR-*slcrb* lines also produced a wide diversity of flower and indeterminate fruit phenotypes, although the presence of fruits with weak or severe mutant phenotypes did not exceed 50%, the percentages of fruits with the severe mutant phenotype close to 15% (Fig. 4c). These results revealed that *SICRCa* and *SICRCb* could have partially redundant roles in FM determinacy.

Taking into account that RNA-seq results showed that *SICRCb* was up-regulated in *fig* floral buds, the question arose as to whether a compensatory mechanism between tomato *CRC* paralogues may be involved in gynoecium determination. For that purpose, *SICRCa* and *SICRCb* expression was quantified in reproductive tissues of *slcrb* and *slerca* CRISPR/Cas9 null mutants, respectively. *SICRCb* was differentially up-regulated in CR-*slerca* floral buds at developmental stages 0–6 (Fig. 4d). *SICRCb* was also up-regulated in CR-*slerca* from floral buds to anthesis day during floral development, whereas *SICRCa* transcripts were up-regulated in CR-*slcrb* floral buds at developmental stages 0–6

(Fig. 4d). Additionally, we generated CR-*slerca:slcrb* double-mutant plants to further dissect the relationship between tomato *CRC* paralogues. Remarkably, the simultaneous loss of function of *SICRCa* and *SICRCb* resulted in homeotic alterations affecting carpel development as the shape of some of its cells attained a stamen-like nature (Figs 4e, S5). CR-*slerca:slcrb* flowers produced stamen-like carpels in a reiterating pattern exclusively affecting the fourth whorl, thus forming fruits with a severe indeterminate phenotype (Fig. 4f,g), which in all cases was considerably more severe than in either CR-*slerca* or CR-*slcrb* single mutants. Hence, complete penetrance and invariable expressivity were found when both tomato paralogues lost their functions.

### Tomato *CRC* paralogues bind to the chromatin remodelling complex members repressing *SIWUS* expression

Floral determinacy requires the repression of the stem cell identity gene *SIWUS* (Bollier *et al.*, 2018); therefore, we further investigated the function of tomato *CRC* paralogues in FM determination by examining the spatio-temporal expression of *SIWUS*. In WT flowers, *SIWUS* expression in the organizing centre was detected from early FM developmental stages (Chu *et al.*, 2019), until stem cell activity was arrested in floral buds at stages 4–5, when the carpel primordia started to emerge (Fig. 5a). From stage 6 onwards, *SIWUS* signal was completely abolished in WT developing carpels. However, *SIWUS* transcripts were detected, between the growing but still unfused carpel primordia, in both CR-*slerca* and CR-*slcrb* floral buds at stage 6. *SIWUS* expression was even observed at later stages in a small group of cells in the placenta, where the initiation of new carpel primordia probably occurs (Fig. 5a). An enlarged *SIWUS* expression domain was observed in CR-*slerca:slcrb* flowers leading to an increased FM size, which agrees with the severe indeterminacy found in double-mutant carpels (Fig. 5a). Hence, the extended expression of *SIWUS* correlates with the floral indeterminacy phenotype of CR-*slerc* lines, suggesting that tomato *CRC* paralogues might participate in the regulation of *SIWUS* transcription limiting FM activity and promoting floral determinacy.

A complete termination of floral stem cell activity in tomato is mediated by a chromatin remodelling complex consisting of SIIMA (Solyc02g087970), SIKNU (Solyc02g160370), SITPL (Solyc01g100050) and SIHDA1 (Solyc09g091440), which enables the repression of *SIWUS* (Bollier *et al.*, 2018). As *SIWUS* expression was misregulated in CR-*slerca* and CR-*slcrb* indeterminate flowers, we wondered whether tomato *CRC* paralogues might be part of this regulatory pathway. Since SIKNU, SIIMA, SITPL1 and SIHDA1 show nuclear localization, we first evaluated SICRCa and SICRCb subcellular localization by transient expression of N-terminal GFP-tagged versions of SICRCa and SICRCb. A confocal microscopy analysis revealed an exclusive nuclear localization for both proteins (Fig. 5b). Next, we conducted BiFC assays to evaluate whether tomato *CRC* paralogues might physically interact *in planta* with the chromatin remodelling complex members including SIKNU, SIIMA, SITPL1 and SIHDA1. As noted by the YFP signal observed at the nucleus of epidermal cells, SICRCa and SICRCb were able to physically

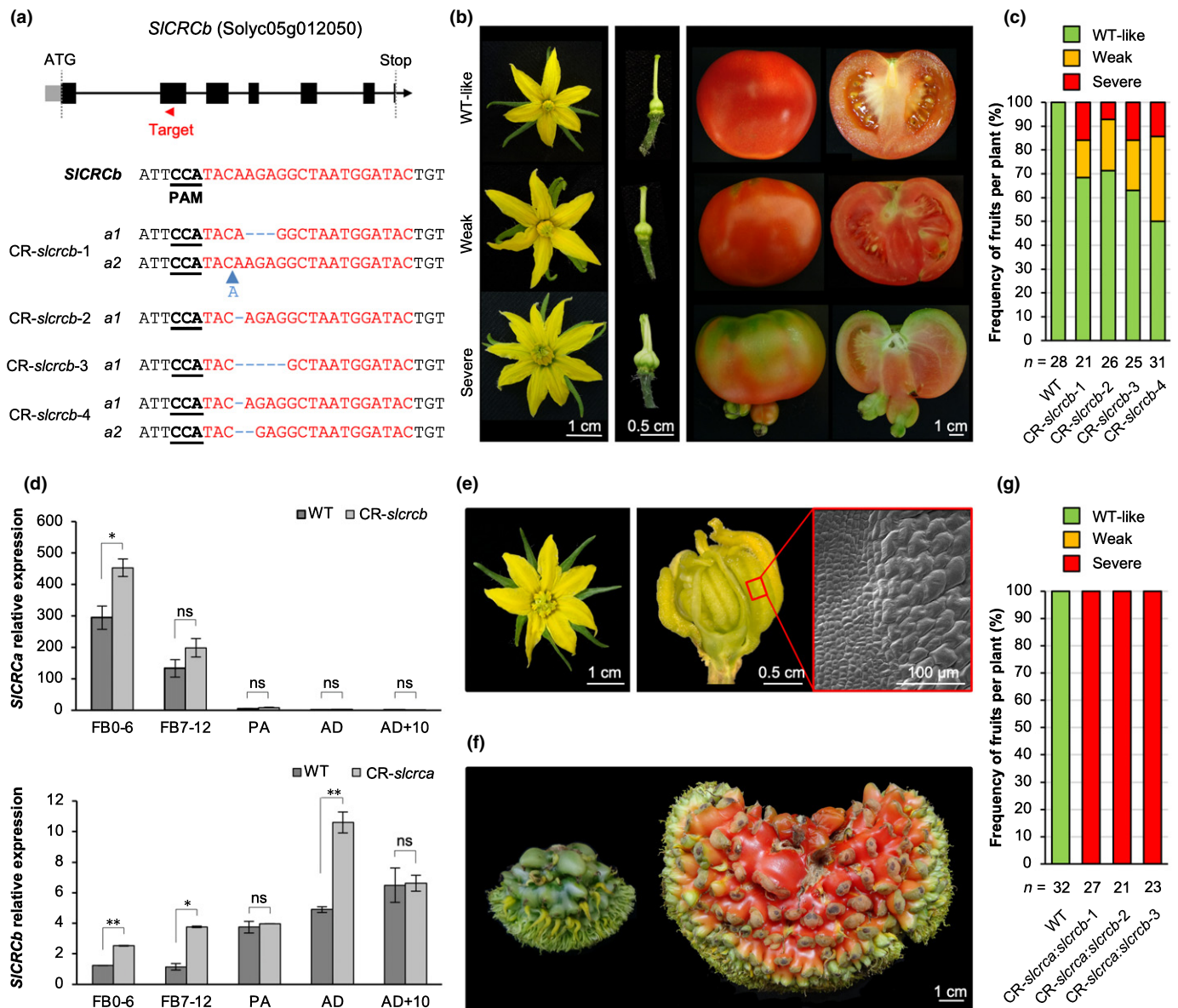


**Fig. 4** Characterization of tomato CRISPR/Cas9-*slcrb* (CR-*slcrb*) and double-mutant CR-*slcrca:slcrb* lines. (a) CR-*slcrb* alleles identified by cloning and sequencing PCR products from the *SICRCb*-targeted region from four T<sub>0</sub> CRISPR plants. Black bold and underlined letters indicate protospacer adjacent motif (PAM) sequences, blue dashed lines show InDel mutations, and blue letter and arrow indicate an insertion sequence. (b) Representative CR-*slcrb* flowers, pistils and fruits exhibiting WT-like (identical to wild-type, WT), weak and severe phenotypes. (c) Percentage of different types of fruits harvested from WT and T<sub>0</sub> CR-*slcrb* plants. (d) Relative expression of *SICRCa* and *SICRCb* in CR-*slcrb* and CR-*slcrca* lines, respectively, at different floral developmental stages. FB0-6, floral buds from stages 0 to 6; FB7-12, floral buds from stages 7 to 12; PA, flowers at pre-anthesis stage; AD, flowers at anthesis stage; and AD+10, flowers 10 d after anthesis stage. Data are means ± SD of three biological and two technical replicates. A two-tailed, two-sample Student *t*-test was performed, and significant differences are represented by asterisks: \*,  $P < 0.01$ ; \*\*,  $P < 0.001$ ; ns, no statistically significant differences. (e, f) Representative flower, pistil and fruits developed by CR-*slcrca:slcrb* double mutants. (e) Detail of the fourth floral whorl organs and morphological features of their epidermal cells in a flower at anthesis stage. (f) Immature green and mature red fruits. (g) Percentage of different types of fruits harvested from WT and T<sub>0</sub> CR-*slcrca:slcrb* plants. In (c, g), *n* value indicates the number of fruits harvested per plant.

interact with each other and each of them in turn with SIKNU, SIIMA and SIHDA1. In addition, SICRCb, but not SICRCa, was found to bind to SITPL1 (Fig. 5c). The lack of interaction between SICRCa and SITPL1 was also confirmed by BiFC experiments in the opposite orientation (Fig. S6). The interactions described above were furthermore corroborated by co-immunoprecipitation (CoIP) studies (Fig. 5d), evidencing that SICRCa and SICRCb can physically bind to the chromatin

remodelling complex members, which in turn repress *SIWUS* expression to promote FM determinacy.

#### Tomato *CRC* paralogues partially rescue the loss of function of the Arabidopsis *CRC* gene

In Arabidopsis, mutations in *CRC* affect gynoecium development, which fails to fuse at the apex, making it wider and shorter

than the WT one (Alvarez & Smyth, 1999; Bowman & Smyth, 1999). As tomato *CRC* paralogues seem to have partially redundant functions, we next questioned whether they may be able to complement the phenotypic defects of Arabidopsis *crc* mutants. Thus, the *crc-1* mutant, a strong hypomorphic allele in the *Ler* genetic background, was genetically transformed with either *SICRCa* or *SICRCb* coding sequences under the control of the Arabidopsis *CRC* promoter (*pCRC::SICRCa* and *pCRC::SICRCb*). For these experiments, a 3860-bp fragment from upstream of the Arabidopsis *CRC* start codon was used as promoter sequence since its functionality has been previously demonstrated (Fourquin *et al.*, 2007). In comparison with WT *Ler* plants, *crc-1* exhibited unfused carpels and the abolition of nectary development, as well as considerably shorter and wider siliques (Fig. 6). The *pCRC::SICRCa* and *pCRC::SICRCb* transgenes were able to fully restore carpel fusion (Fig. 6c) and slightly increased silique length (Fig. 6a,b). In agreement with the lack of nectaries in tomato flowers, *SICRCa* and *SICRCb* did not rescue nectary development in *crc-1* (Fig. 6d). As a control, WT *Ler* plants were also transformed with either *pCRC::SICRCa* or *pCRC::SICRCb*, which exhibited no significant differences with respect to untransformed *Ler* plants (Fig. S7). Overall, our results denote that tomato *CRC* paralogues are capable of partially restoring a WT phenotype when transformed into *crc-1* plants.

## Discussion

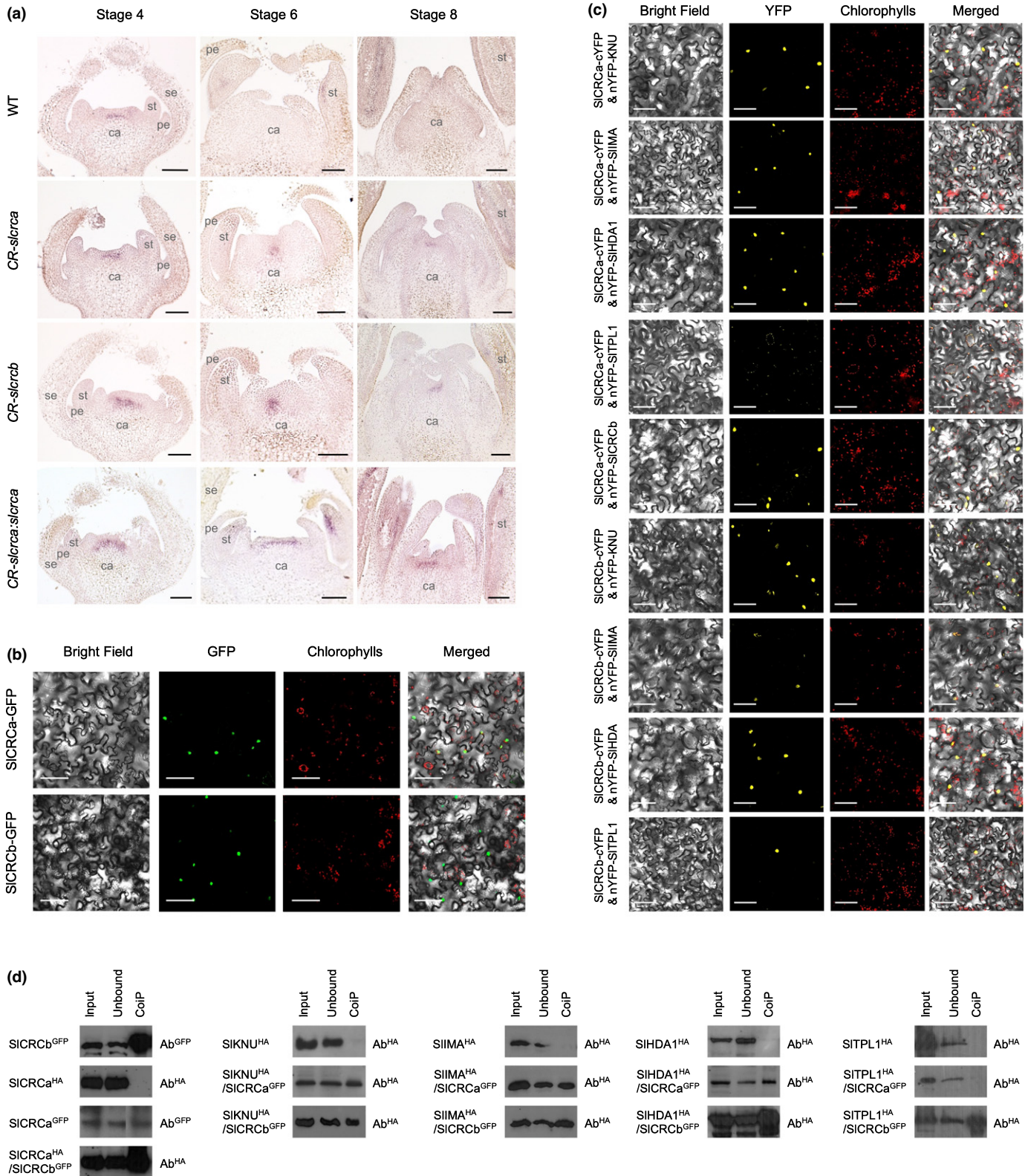
### Tomato *CRC* paralogues safeguard floral determinacy by acting in a partially redundant and compensatory manner

We have addressed the functional characterization of tomato paralogous *CRC* genes and examined their potential roles in FM determinacy and carpel formation. Our results revealed that a 367-bp insertion in the fourth intron of the *SICRCa* gene causes the carpel-inside-carpel phenotype observed in *fig* plants. Loss-of-function analyses of *SICRCa*, involving either knockdown or knockout approaches, allowed for the generation of an allelic series at this locus, which resulted in analogous mutant phenotypes with incomplete penetrance and variable expressivity. Indeed, variable floral and fruit phenotypes were observed even in the same individual, ranging from indistinguishable from WT to severe developmental defects. Consequently, these results denoted that any impairment of *SICRCa* function would give rise to a loss of FM determinacy characterized by the proliferation of additional carpels within the unfused primary carpels. Our results also suggested that there is not a direct correlation between *SICRCa* mRNA levels and the severity of the mutant phenotypes, which agrees with the hypothesis that proposes a nonlinear gene dosage response for developmental regulators involved in complex transcriptional regulatory networks (Birchler *et al.*, 2016). The lack of predictability between gene dosage and phenotypic alterations has been also reported for other tomato meristem genes. Thus, through creating a series of cis-regulatory alleles by genome editing, Rodríguez-Leal *et al.* (2017) demonstrated that variations in fruit size are not predicted by changes in gene expression levels of the CLAVATA-WUSCHEL pathway.

Incomplete penetrance and variable expressivity of mutant phenotypes were also observed among knockout mutant lines for *SICRCb*, whereas all flowers developed by double-mutant plants for *SICRCa* and *SICRCb* loci showed a severe indeterminate phenotype. Based on these results, we conclude that tomato *CRC* paralogues operate as positive regulators of floral determinacy by acting in a partially redundant manner to safeguard normal determination of FM and carpel development. Indeed, the loss of carpel identity in the CR-*slcrca:slcrb* double mutant supports the role of tomato *CRC* paralogues in establishing carpel identity for proper completion of gynoecium and fruit developmental programmes. Furthermore, *SICRCa* was differentially up-regulated in tomato floral buds lacking *SICRCb* function, and vice versa, *SICRCb* expression significantly increased in the absence of *SICRCa* activity. Therefore, an active compensation mechanism of *SICRCa* and *SICRCb* functions may participate in the regulation of FM determinacy. In support of this hypothesis, transcriptional compensation has been recently described as a means to control meristematic activity in tomato, where the CLV3/embryo-surrounding region (CLE) ligand paralogues operate to buffer stem cell homeostasis (Rodríguez-Leal *et al.*, 2019). Hence, the absence of *SICRCa* or *SICRCb* gene function would trigger an active compensation mechanism involving the up-regulation of *SICRCb* or *SICRCa*, respectively, which help to buffer the severity of flower developmental alterations. However, environmental or other genetic factors could lead to a partially compensatory response influencing penetrance and expressivity of phenotypes associated with single mutations at either *SICRCa* or *SICRCb* loci. Altogether, our results indicate that tomato *CRC* paralogues operate as positive regulators of FM determinacy by acting in a partially redundant and compensatory manner to ensure normal floral development.

### Evolutionary conservation and divergence of *CRC* gene function in tomato

The role of putative *CRC* orthologues in FM determinacy and gynoecium development seems to have been conserved across angiosperms (Bowman & Smyth, 1999; Yamaguchi *et al.*, 2004; Fourquin *et al.*, 2005, 2007, 2014; Lee *et al.*, 2005a,b; Nakayama *et al.*, 2010; Bartholmes *et al.*, 2012; Sun *et al.*, 2013; Morel *et al.*, 2018). Nevertheless, specialized functions of *CRC*-like genes have been acquired after the evolutionary divergence of their respective plant lineages. Thus, in monocot species such as rice, the *CRC* orthologue *DROOPING LEAF (DL)* is also involved in carpel organ identity and plays an essential role in leaf midrib formation, functions that are shared by *CRC* orthologues from other monocot species (Yamaguchi *et al.*, 2004; Ishikawa *et al.*, 2009; Wang *et al.*, 2009; Nakayama *et al.*, 2010; Strable *et al.*, 2017). Likewise, novel functions in stigmatic cavity formation and ovule initiation have been proposed for the paralogous *CRC* genes *PeDL1* and *PeDL2* of the orchid *Phalaenopsis equestris* (Chen *et al.*, 2021). Within the Solanaceae family, the functional role of *CRC* paralogues has also been addressed in petunia, where *PhCRC1* and *PhCRC2* genes, in addition to regulating floral determinacy and carpel development, are required for nectary



development acting in a redundant manner to trigger its formation (Morel *et al.*, 2018). *PhCRC1* and *PhCRC2* showed quasi-identical expression profiles, which displayed an accumulation of their transcripts in carpel primordia, ovary walls, and style and

stigma (Morel *et al.*, 2018), similar to the pattern observed for the tomato *CRC* paralogues at the beginning of flower development. However, although tomato *CRC* paralogues play partially redundant roles to ensure normal floral development, they were

**Fig. 5** Tomato CRC paralogues interact with the chromatin remodelling complex members repressing *SIWUS* expression. (a) *In situ* mRNA hybridization of *SIWUS* in histological sections of wild-type (WT), *CR-slcra*, *CR-slcrb* and *CR-slcra:slcrb* flowers at developmental stages 4, 6 and 8. (b) Subcellular localization of SICRCa and SICRCb. The entire *SICRCa* and *SICRCb* coding sequences were N-terminally fused to green fluorescent protein (GFP) and transiently expressed in *Nicotiana benthamiana* leaves. (c) Bimolecular fluorescence complementation confocal images showing *in vivo* interactions in *N. benthamiana* leaves between either the yellow fluorescent protein (YFP) C-terminal region fused to SICRCa (SICRCa-cYFP) or SICRCb (SICRCb-cYFP), and fusions of the YFP N-terminal region fused to SIKNU (nYFP-SIKNU), SIIMA (nYFP-SIIMA), SIHDA1 (nYFP-SIHDA1) or SITPL1 (nYFP-SITPL1). The SICRCa-cYFP fusion was also examined with SICRCb fused to the YFP N-terminal region (nYFP-SICRCb). As negative control, each protein under study was co-infiltrated with the nonplant  $\beta$ -glucuronidase (GUS) enzyme fused to cYFP or nYFP. No YFP signal was observed in negative controls (Supporting Information Fig. S6). (d) Co-immunoprecipitation studies of *N. benthamiana* leaves expressing either GFP-tagged SICRCa (SICRCa<sup>GFP</sup>) or SICRCb (SICRCb<sup>GFP</sup>) and the different hemagglutinin (HA)-tagged members of the chromatin remodelling complex (SIKUN<sup>HA</sup>, SIIMA<sup>HA</sup>, SIHDA1<sup>HA</sup> or SITPL1<sup>HA</sup>). SICRCb<sup>GFP</sup> was also tested with HA-tagged SICRCa (SICRCa<sup>HA</sup>). The input total protein extracts were immunoprecipitated with anti-GFP beads, and the unbound and recovered fractions (CoIP) were incubated with anti-GFP (Ab<sup>GFP</sup>) and anti-HA (Ab<sup>HA</sup>) antibodies to detect precipitated and co-purified proteins, respectively. In (a), the floral organ primordia of sepal (se), petal (pe), stamen (st) and carpel (ca) are indicated. Bars, 100  $\mu$ m.

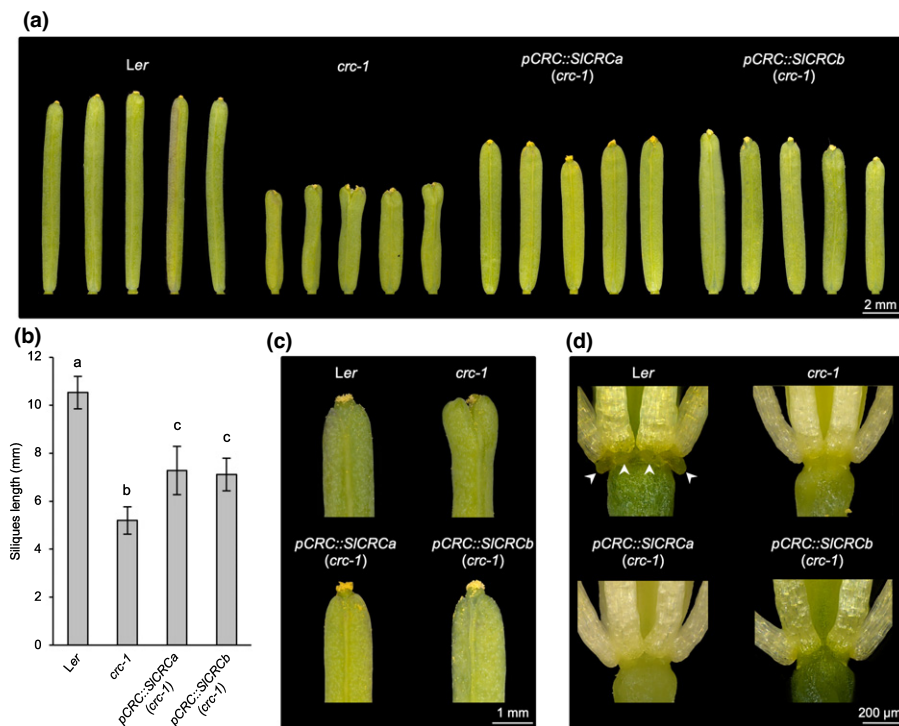


**Fig. 6** Complementation of the Arabidopsis *crc-1* mutation by transformation with tomato *CRC* paralogues. (a–d) Fully elongated siliques (a), silique length (b), silique apices showing different degrees of carpel fusion (c) and development of nectaries (arrows) at the base of the third floral whorl in the Ler wild-type, which are absent in *crc-1* mutant and transgenic *pCRC::SICRCa* and *pCRC::SICRCb* plants (d). In (b), pairwise comparisons of means using the least significant difference test were performed. Values followed by the same lower-case letter are not statistically different ( $P < 0.05$ ). Error bars represent the SD of the mean values.

differentially expressed during flower ontogenesis. Thus, *SICRCa* was mainly expressed at the first stage of the flower bud formation, whereas *SICRCb* transcripts were detected from young floral buds to flowers at 10 d post-anthesis, suggesting that their regulatory elements may have diverged. In summary, although fine-tuning gene regulation events may have favoured gene paralogue speciation, flower and fruit phenotypes of tomato plants lacking *SICRCa* and *SICRCb*, together with gene expression analyses, provide sufficient evidence about the conserved function of these genes in regulating carpel development and floral determinacy. Indeed, the heterologous expression of either *SICRCa* or *SICRCb* genes in Arabidopsis *crc-1* background was capable of partially restoring a WT phenotype, supporting the evolutionary ancestral

role of *CRC*-like genes in promoting floral stem cell termination and carpel formation. However, tomato *CRC* paralogues were not able to rescue the proper formation of nectaries. Previous studies have reported that *CRC* gene functions in nectary development appear to be conserved in several core eudicot species, whereas *CRC*-like genes are not required for nectary formation in basal angiosperms, which would support the hypothesis that *CRC* function in nectary specification may be the consequence of *CRC* neofunctionalization within diverse lineages of core eudicots (Fourquin *et al.*, 2005, 2014; Lee *et al.*, 2005b; Yamada *et al.*, 2011).

In Arabidopsis and rice, *CRC* orthologue genes have also been found to act antagonistically with class B genes in promoting

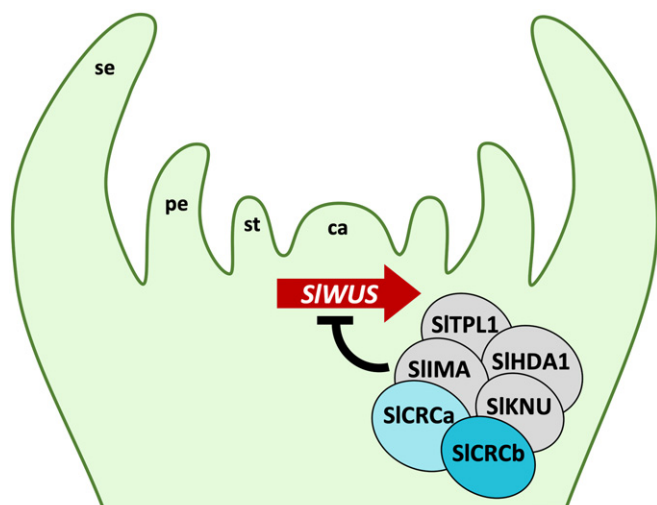


**Fig. 7** Proposed model for the function of tomato CRC paralogs in *SIWUS* repression and the floral meristem determinacy. Tomato CRC paralogs (*SICRCa* and *SICRCb*), *SIIMA* and *SIKNU* interact with *SIHDA1* and *SITPL1* to form a chromatin remodelling complex that represses *SIWUS* expression to terminate floral stem cell activity once carpel primordia are initiated. The blunt-ended arrow indicates regulatory repression of gene expression. se, sepal; pe, petal; st, stamen; and ca, carpel.

carpel development (Alvarez & Smyth, 1999; Bowman & Smyth, 1999; Yamaguchi *et al.*, 2004). Here, we found that double mutant plants for *SICRCa* and *SICRCb* loci develop flowers with stamen-like carpels growing in a reiterating pattern inside the fourth whorl, which strongly hints that tomato CRC paralogs seem to have common functions with the Arabidopsis and rice counterparts as negative regulators of class B genes. Accordingly, a recent research in the Solanaceae family member *Physalis floridana* has revealed regulatory and genetic interactions between B-class MADS-box and *CRC* genes in a context-dependent manner during flower development (Gong *et al.*, 2021).

Tomato CRC paralogs are part of the chromatin remodelling complex that represses *SIWUS* in floral meristems

A complex regulatory network involving signalling cascades, transcriptional regulation, epigenetic mechanisms and hormonal control for FM determinacy has been described in Arabidopsis (Shang *et al.*, 2019). Thus, the function of *CRC* as regulator of floral determinacy has hitherto been limited to modulate auxin homeostasis by both activating *YUC4* and repressing *TRN2* gene expression (Yamaguchi *et al.*, 2017, 2018). Our findings reveal a new role for tomato *CRC* paralogs in balancing floral stem cell proliferation and differentiation, as they can physically bind to the members of the chromatin remodelling complex that drives the epigenetic regulation of *SIWUS* expression. In this epigenetic silencing mechanism, *SIIMA* acts as an adaptor protein engaging *SIKNU* in a complex that involves *SITPL* and *SIHDA1* leading to *SIWUS* repression (Bollier *et al.*, 2018). Based on the *SIWUS* expression profiles in flowers of single and double mutants for

*SICRCa* and *SICRCb*, as well as protein interaction data hereby reported, it seems reasonable to propose a model by which *SICRCa* and *SICRCb* would act in specifying floral determinacy by binding to the chromatin remodelling complex that ensures the proper spatio-temporal repression of *SIWUS* during flower development (Fig. 7). A future challenge will be to assess the role of tomato *CRC* paralogs in regulating auxin homeostasis, as well as to determine whether *CRC* interactions are conserved in angiosperm species. Further studies on the degree of conservation or divergence in the molecular mechanism triggering floral determinacy will provide valuable information for crop yield improvement, as the number of carpels in a flower, and consequently the final number of locules forming the mature fruit, plays a key role in regulating fruit size and external fruit quality, important traits in breeding programmes. In conclusion, this research contributes to the ever-increasing understanding of meristem regulatory pathways that will allow for the development of new knowledge-driven breeding strategies, whose implementation will in turn significantly contribute to the sustainability of agriculture in the coming decades.

## Acknowledgements

This work was supported by the PID2019-110833RB-C31 and PID2019-110833RB-C32 grants from the Spanish Ministry of Science and Innovation (MICI/AEI/FEDER, UE) and the BRESOV (Breeding for Resilient, Efficient and Sustainable Organic Vegetable production) project funding by the Research and Innovation Programme of the European Union Horizon 2020 (grant agreement no. 774244). The authors thank Cristina Ferrándiz for critical review of the manuscript. The authors also thank research facilities provided by the Campus de Excelencia Internacional Agroalimentario (CeIA3).

## Author contributions

LC performed most experimental procedures, prepared figures and co-wrote the manuscript. EG, BP, BG-S, AO-A and RM-P participated in the experimental research. TA, JC, VM, FJY-L and RL contributed materials and genetic resources and analysed data. FJY-L and RL conceived and supervised research and co-wrote the paper.

## ORCID

Trinidad Angosto <https://orcid.org/0000-0003-0294-9255>  
 Juan Capel <https://orcid.org/0000-0002-4327-0604>  
 Laura Castañeda <https://orcid.org/0000-0002-0314-0696>  
 Estela Giménez <https://orcid.org/0000-0002-7403-5279>  
 Rafael Lozano <https://orcid.org/0000-0001-5458-2075>  
 Rosa Micol-Ponce <https://orcid.org/0000-0001-9389-2906>  
 Vicente Moreno <https://orcid.org/0000-0002-0345-7300>  
 Ana Ortiz-Atienza <https://orcid.org/0000-0003-1750-4785>  
 Benito Pineda <https://orcid.org/0000-0001-9176-701X>  
 Fernando J. Yuste-Lisbona <https://orcid.org/0000-0001-9222-7293>

## Data availability

Tomato sequence data from this article can be found at the SOL Genomics Network (SGN; <https://solgenomics.net/>) under accession nos. Solyc01g010240 (*SlCRCA*), Solyc05g012050 (*SlCRCB*), Solyc02g083950 (*SlWUS*), Solyc02g087970 (*SlIMA*), Solyc02g160370 (*SlKNU*), Solyc01g100050 (*SlTPL*) and Solyc09g091440 (*SlHDA1*). The sequence data from Arabidopsis can be found at the Arabidopsis Information Resource (TAIR; <https://www.arabidopsis.org/>) under the accession no. At1g69180 (*CRC*). The DNA-seq and RNA-seq data from this article can be found at the Sequence Read Archive (SRA; <https://www.ncbi.nlm.nih.gov/sra/>) under BioProject accession nos. PRJNA685617 and PRJNA686085, respectively.

## References

- Alvarez J, Smyth DR. 1999. *CRABS CLAW* and *SPATULA*, two Arabidopsis genes that control carpel development in parallel with *AGAMOUS*. *Development* 126: 2377–2386.
- Bartholmes C, Hidalgo O, Gleissberg S. 2012. Evolution of the *YABBY* gene family with emphasis on the basal eudicot *Eschscholzia californica* (Papaveraceae). *Plant Biology* 14: 11–23.
- Birchler JA, Johnson AF, Veitia RA. 2016. Kinetics genetics: incorporating the concept of genomic balance into an understanding of quantitative traits. *Plant Science* 245: 128–134.
- Bollier N, Sicard A, Leblond J, Latrasse D, Gonzalez N, Gévaudant F, Benhamed M, Raynaud C, Lenhard M, Chevalier C *et al.* 2018. At-MINI ZINC FINGER2 and SI-INHIBITOR OF MERISTEM ACTIVITY, a conserved missing link in the regulation of floral meristem termination in Arabidopsis and tomato. *Plant cell* 30: 83–100.
- Bowman JL, Smyth DR. 1999. *CRABS CLAW*, a gene that regulates carpel and nectary development in Arabidopsis, encodes a novel protein with zinc finger and helix-loop-helix domains. *Development* 126: 2387–2396.
- Brukhin V, Hernould M, Gonzalez N, Chevalier C, Mouras A. 2003. Flower development schedule in tomato *Lycopersicon esculentum* cv. sweet cherry. *Sexual Plant Reproduction* 15: 311–320.
- Chen YY, Hsiao YY, Li CI, Yeh CM, Mitsuda N, Yang HX, Chiu CC, Chang SB, Liu ZJ, Tsai WC. 2021. The ancestral duplicated *DL/CRC* orthologs, *PeDL1* and *PeDL2*, function in orchid reproductive organ innovation. *Journal of Experimental Botany* 72: 5442–5461.
- Chu Y, Jang J, Huang Z, van der Knaap E. 2019. Tomato locule number and fruit size controlled by natural alleles of *lc* and *fas*. *Plant Direct* 3: e00142.
- Clough SJ, Bent AF. 1998. Floral dip: a simplified method for *Agrobacterium*-mediated transformation of *Arabidopsis thaliana*. *The Plant Journal* 16: 735–743.
- Ditta G, Pinyopich A, Robles P, Pelaz S, Yanofsky MF. 2004. The *SEP4* gene of *Arabidopsis thaliana* functions in floral organ and meristem identity. *Current Biology* 14: 1935–1940.
- Ellul P, Garcia-Sogo B, Pineda B, Ríos G, Roig LA, Moreno V. 2003. The ploidy level of transgenic plants in *Agrobacterium*-mediated transformation of tomato cotyledons (*Lycopersicon esculentum* Mill.) is genotype and procedure dependent. *Theoretical and Applied Genetics* 106: 231–238.
- Fourquin C, Primo A, Martínez-Fernández I, Huet-Trujillo E, Ferrándiz C. 2014. The *CRC* orthologue from *Pisum sativum* shows conserved functions in carpel morphogenesis and vascular development. *Annals of Botany* 114: 1535–1544.
- Fourquin C, Vinauger-Douard M, Chambrier P, Berne-Dedieu A, Scutt CP. 2007. Functional conservation between *CRABS CLAW* orthologues from widely diverged angiosperms. *Annals of Botany* 100: 651–657.
- Fourquin C, Vinauger-Douard M, Fogliani B, Dumas C, Scutt CP. 2005. Evidence that *CRABS CLAW* and *TOUSLED* have conserved their roles in carpel development since the ancestor of the extant angiosperms. *Proceedings of the National Academy of Sciences, USA* 102: 4649–4654.
- Gleave AP. 1992. A versatile binary vector system with a T-DNA organisational structure conducive to efficient integration of cloned DNA into the plant genome. *Plant Molecular Biology* 20: 1203–1207.
- Gong P, Song C, Liu H, Li P, Zhang M, Zhang J, Zhang S, He C. 2021. *PFCRC* mediates neofunctionalization of *Physalis GLOBOSA* genes in carpel development. *Journal of Experimental Botany* 72: 6882–6903.
- Gremski K, Ditta G, Yanofsky MF. 2007. The *HECATE* genes regulate female reproductive tract development in *Arabidopsis thaliana*. *Development* 134: 3593–3601.
- Guo L, Cao X, Liu Y, Li J, Li Y, Li D, Zhang K, Gao C, Dong A, Liu X. 2018. A chromatin loop represses *WUSCHEL* expression in Arabidopsis. *The Plant Journal* 94: 1083–1097.
- Ishikawa M, Ohmori Y, Tanaka W, Hirabayashi C, Murai K, Ogihara Y, Yamaguchi T, Hirano HY. 2009. The spatial expression patterns of *DROOPING LEAF* orthologs suggest a conserved function in grasses. *Genes & Genetic Systems* 84: 137–146.
- Kim D, Pertea G, Trapnell C, Pimentel H, Kelley R, Salzberg SL. 2013. TOPHAT2: accurate alignment of transcriptomes in the presence of insertions, deletions and gene fusions. *Genome Biology* 14: R36.
- Krizek BA, Fletcher JC. 2005. Molecular mechanisms of flower development: an armchair guide. *Nature Reviews Genetics* 6: 688–698.
- Kwon CS, Chen C, Wagner D. 2005. *WUSCHEL* is a primary target for transcriptional regulation by *SPLAYED* in dynamic control of stem cell fate in Arabidopsis. *Genes & Development* 19: 992–1003.
- Langmead B, Salzberg SL. 2012. Fast gapped-read alignment with BOWTIE2. *Nature Methods* 9: 357–359.
- Lawrence M, Huber W, Pagès H, Aboyoun P, Carlson M, Gentleman R, Morgan MT, Carey VJ. 2013. Software for computing and annotating genomic ranges. *PLoS Computational Biology* 9: e1003118.
- Lee JY, Baum SF, Alvarez J, Patel A, Chitwood DH, Bowman JL. 2005a. Activation of *CRABS CLAW* in the nectaries and carpels of Arabidopsis. *Plant cell* 17: 25–36.
- Lee JY, Baum SF, Oh SH, Jiang CZ, Chen JC, Bowman JL. 2005b. Recruitment of *CRABS CLAW* to promote nectary development within the eudicot clade. *Development* 132: 5021–5032.
- Liu X, Kim YJ, Müller R, Yumul RE, Liu C, Pan Y, Cao X, Goodrich J, Chen X. 2011. *AGAMOUS* terminates floral stem cell maintenance in Arabidopsis by directly repressing *WUSCHEL* through recruitment of Polycomb Group Proteins. *Plant cell* 23: 3654–3670.
- Love MI, Huber W, Anders S. 2014. Moderated estimation of fold change and dispersion for RNA-seq data with DESeq2. *Genome Biology* 15: 550.
- Lozano R, Angosto T, Gómez P, Payan C, Capel J, Huijser P, Salinas J, Martínez-Zapater JM. 1998. Tomato flower abnormalities induced by low temperatures are associated with changes of expression of MADS-Box genes. *Plant Physiology* 117: 91–100.
- Morel P, Heijmans K, Ament K, Choppy M, Trehin C, Chambrier P, Rodrigues Bento S, Bimbo A, Vandebussche M. 2018. The floral C-lineage genes trigger nectary development in petunia and Arabidopsis. *Plant cell* 30: 2020–2037.
- Nakagawa T, Kurose T, Hino T, Tanaka K, Kawamukai M, Niwa Y, Toyooka K, Matsuoka K, Jinbo T, Kimura T. 2007. Development of series of gateway binary vectors, pGWBs, for realizing efficient construction of fusion genes for plant transformation. *Journal of Bioscience and Bioengineering* 104: 34–41.
- Nakayama H, Yamaguchi T, Tsukaya H. 2010. Expression patterns of *AaDL*, a *CRABS CLAW* ortholog in *Asparagus asparagoides* (Asparagaceae), demonstrate a stepwise evolution of *CRC/ DL* subfamily of *YABBY* genes. *American Journal of Botany* 97: 591–600.
- Oliveros JC, Franch M, Tabas-Madrid D, San-León D, Montoliu L, Cubas P, Pazos F. 2016. Breaking-Cas—interactive design of guide RNAs for CRISPR-Cas experiments for ENSEMBL genomes. *Nucleic Acids Research* 44: W267–W271.
- Pérez-Martín F, Yuste-Lisbona FJ, Pineda B, Angarita-Díaz MP, García-Sogo B, Antón T, Sánchez S, Giménez E, Atarés A, Fernández-Lozano A *et al.* 2017. A collection of enhancer trap insertional mutants for functional genomics in tomato. *Plant Biotechnology Journal* 15: 1439–1452.
- Phukela B, Geeta R, Das S, Tandon R. 2020. Ancestral segmental duplication in Solanaceae is responsible for the origin of *CRCa-CRCb* paralogues in the family. *Molecular Genetics and Genomics* 295: 563–577.

- R Development Core Team. 2020. *R: a language and environment for statistical computing, v.4.0.1*. Vienna, Austria: R Foundation for Statistical Computing. [WWW document] URL <https://www.r-project.org/>.
- Rodríguez-Leal D, Lemmon ZH, Man J, Bartlett ME, Lippman ZB. 2017. Engineering quantitative trait variation for crop improvement by genome editing. *Cell* 171: 470–480.e8.
- Rodríguez-Leal D, Xu C, Kwon C-T, Soyars C, Demesa-Arevalo E, Man J, Liu L, Lemmon ZH, Jones DS, Van Eck J *et al.* 2019. Evolution of buffering in a genetic circuit controlling plant stem cell proliferation. *Nature Genetics* 51: 786–792.
- Shang E, Ito T, Sun B. 2019. Control of floral stem cell activity in Arabidopsis. *Plant Signaling & Behavior* 14: 1659706.
- Strable J, Wallace JG, Unger-Wallace E, Briggs S, Bradbury PJ, Buckler ES, Vollbrecht E. 2017. Maize *YABBY* genes *drooping leaf1* and *drooping leaf2* regulate plant architecture. *Plant Cell* 29: 1622–1641.
- Sun B, Ito T. 2015. Regulation of floral stem cell termination in Arabidopsis. *Frontiers in Plant Science* 6: 17.
- Sun B, Looi LS, Guo S, He Z, Gan ES, Huang J, Xu Y, Wee WY, Ito T. 2014. Timing mechanism dependent on cell division is invoked by polycomb eviction in plant stem cells. *Science* 343: 1248559.
- Sun B, Xu Y, Ng KH, Ito T. 2009. A timing mechanism for stem cell maintenance and differentiation in the Arabidopsis floral meristem. *Genes & Development* 23: 1791–1804.
- Sun B, Zhou Y, Cai J, Shang E, Yamaguchi N, Xiao J, Looi LS, Wee WY, Gao X, Wagner D *et al.* 2019. Integration of transcriptional repression and polycomb-mediated silencing of *WUSCHEL* in floral meristems. *Plant Cell* 31: 1488–1505.
- Sun W, Huang W, Li Z, Lv H, Huang H, Wang Y. 2013. Characterization of a *CRABS CLAW* gene in basal eudicot species *Epimedium sagittatum* (Berberidaceae). *International Journal of Molecular Sciences* 14: 1119–1131.
- Tian T, Liu Y, Yan H, You Q, Yi X, Du Z, Xu W, Su Z. 2017. agriGO v.2.0: a GO analysis toolkit for the agricultural community, 2017 update. *Nucleic Acids Research* 45: W122–W129.
- Vazquez-Vilar M, Bernabé-Orts JM, Fernandez-Del-Carmen A, Ziarsolo P, Blanca J, Granell A, Orzaez D. 2016. A modular toolbox for gRNA–Cas9 genome engineering in plants based on the GoldenBraid standard. *Plant Methods* 12: 10.
- Wang A, Tang J, Li D, Chen C, Zhao X, Zhu L. 2009. Isolation and functional analysis of *LiYAB1*, a *YABBY* family gene, from lily (*Lilium longiflorum*). *Journal of Plant Physiology* 166: 988–995.
- Wesley SV, Helliwell CA, Smith NA, Wang MB, Rouse DT, Liu Q, Gooding PS, Singh SP, Abbott D, Stoutjesdijk PA *et al.* 2001. Construct design for efficient, effective and high-throughput gene silencing in plants. *The Plant Journal* 27: 581–590.
- Winer J, Jung CKS, Shackel I, Williams PM. 1999. Development and validation of real-time quantitative reverse transcriptase–polymerase chain reaction for monitoring gene expression in cardiac myocytes *in vitro*. *Analytical Biochemistry* 270: 41–49.
- Yamada T, Yokota S, Hirayama Y, Imaichi R, Kato M, Gasser CS. 2011. Ancestral expression patterns and evolutionary diversification of *YABBY* genes in angiosperms. *The Plant Journal* 67: 26–36.
- Yamaguchi N, Huang J, Tatsumi Y, Abe M, Sugano SS, Kojima M, Takebayashi Y, Kiba T, Yokoyama R, Nishitani K *et al.* 2018. Chromatin-mediated feed-forward auxin biosynthesis in floral meristem determinacy. *Nature Communications* 9: 5290.
- Yamaguchi N, Huang J, Xu Y, Tanoi K, Ito T. 2017. Fine-tuning of auxin homeostasis governs the transition from floral stem cell maintenance to gynoecium formation. *Nature Communications* 8: 1125.
- Yamaguchi T, Nagasawa N, Kawasaki S, Matsuoka M, Nagato Y, Hirano HY. 2004. The *YABBY* gene *DROOPING LEAF* regulates carpel specification and midrib development in *Oryza sativa*. *Plant Cell* 16: 500–509.
- Yuste-Lisbona FJ, Fernández-Lozano A, Pineda B, Bretones S, Ortiz-Atienza A, García-Sogo B, Müller NA, Angosto T, Capel J, Moreno V *et al.* 2020. *ENO* regulates tomato fruit size through the floral meristem development network. *Proceedings of the National Academy of Sciences, USA* 117: 8187–8195.
- Yuste-Lisbona FJ, Jiménez-Gómez JM, Capel C, Lozano R. 2021. Effective mapping by sequencing to isolate causal mutations in the tomato genome. *Methods in Molecular Biology* 2264: 89–103.

## Supporting Information

Additional Supporting Information may be found online in the Supporting Information section at the end of the article.

**Fig. S1** Phenotypic details of *fig* pistils and fruits.

**Fig. S2** Southern blot and PCR assays of *fig* plants.

**Fig. S3** Gene ontology term enrichment analysis.

**Fig. S4** Microsynteny conservation analyses between genomic blocks containing *CRC* genes in Arabidopsis and tomato.

**Fig. S5** Scanning electron micrograph images showing homeotic alterations in flower development of CR-*slcrca:slcreb* double mutant plants.

**Fig. S6** Bimolecular fluorescence complementation assays on *Nicotiana benthamiana* leaves.

**Fig. S7** Transformation of Arabidopsis wild-type *Ler* plants with tomato *CRC* paralogues.

**Methods S1** Plant material and growth conditions.

**Methods S2** Optical microscopy and scanning electron microscopy analyses.

**Table S1** Primer sequences used for *SICRCA* genotyping, RNAi and CRISPR/Cas9 assays.

**Table S2** Primer sequences used for expression analyses.

**Table S3** Primer sequences used for *Arabidopsis thaliana* mutant complementation constructs.

**Table S4** Primer sequences used for cloning into the entry vector pENTR/D-TOPO the coding sequences of genes tested for sub-cellular localization and protein–protein interaction assays.

**Table S5** Floral organ number and fruit characteristics of *fig* mutant plants.

**Table S6** Significantly differentially expressed gene list ( $P_{adj} < 0.05$ ) for *fig* floral buds compared to wild-type ones.

**Table S7** Functional GO enrichment analysis of differentially expressed genes for *fig* floral buds compared to wild-type ones.

Please note: Wiley Blackwell are not responsible for the content or functionality of any Supporting Information supplied by the authors. Any queries (other than missing material) should be directed to the *New Phytologist* Central Office.